CrystEngComm

HIGHLIGHT

Wadsley vanadium oxides

Andrzej Grzechnik [iD] *[ab] and Karen Friese[bc]

Wadsley vanadium oxides form a homologous series V_nO_{2n+1} between the end members α-V_2O_5 and VO_2(B). They exhibit a variety of crystal structures due to different polyhedra around the V^{4+} and V^{5+} cations and polyhedral connectivity. Their structural features as well as transport and magnetic properties are reviewed here. The Wadsley vanadium oxides are oxygen deficient with different ordered vacancies in the oxygen cubic close-packing array. The rutile-type structure, with the oxygen hexagonal close packing, is found in V_6O_{13} ($n = 6$) obtained at high pressures and high temperatures, which unlike its α polymorph stable at atmospheric conditions, does not undergo a metal–insulator phase transition. This finding opens a possibility of synthesizing new materials with unexpected properties in the system V_2O_5–VO_2 by varying compositions and exerting extreme conditions.

Introduction

Experimentally determined equilibrium phases in the central part of the V–O phase diagram (VO_x, $1.5 \leq x \leq 2.5$) at atmospheric pressure are V_2O_3, V_nO_{2n-1} ($n = 3 \div 8$), VO_2, V_3O_7, V_6O_{13}, and V_2O_5, with V_2O_3, VO_2, and V_2O_5 exhibiting very narrow composition ranges.[1] The theoretically calculated phase diagram includes only V_2O_3, V_3O_5, VO_2, V_3O_7, and V_2O_5.[2] The synthesis, functionalities, and applications of the VO_x oxides are extensively reviewed in ref. 2–5.

The oxides V_nO_{2n-1} ($n = 3 \div 9$) form a *Magnéli* homologous series, $V_nO_{2n-1} = V_2O_3 + (n - 2) VO_2$.[6,7] The end members of

this series are corundum-type V_2O_3 and rutile-type VO_2.[8] The corundum structure ($R\bar{3}c$, $Z = 6$) is a hexagonal close-packed array of oxygen atoms, in which the V^{3+} cations occupy two-thirds of the octahedral sites. It is built of pairs of VO_6 octahedra sharing faces along the c direction. Such pairs form chains by edge-sharing in the plane perpendicular to c. These chains are linked to others by edge sharing in a three-dimensional network. The rutile structure (phase R, $P4_2/mnm$, $Z = 2$) is a distorted hexagonal close-packed oxygen array with the V^{4+} cations occupying one half of the octahedral sites. Chains of edge-sharing VO_6 octahedra along the c direction connect with each other in a three-dimensional network. *Magnéli* phases could be derived from the parent rutile structure by removing an oxygen layer at every nth vanadium layer in the direction perpendicular to the (211) plane of the parent rutile structure.[8] With respect to the composition of vanadium dioxide, they are anion deficient and can be expressed as VO_{2-y}. They order antiferromagnetically and,

[a] *Jülich Centre for Neutron Science-4 (JCNS-4), Forschungszentrum Jülich GmbH, Jülich D-52425, Germany. E-mail: a.grzechnik@fz-juelich.de*
[b] *Institute of Crystallography, RWTH Aachen University, Aachen 52056, Germany*
[c] *Jülich Centre for Neutron Science-2 (JCNS-2), Forschungszentrum Jülich GmbH, Jülich D-52425, Germany*

Andrzej Grzechnik studied geology (MSc) at the University of Warsaw and chemistry (PhD) at Arizona State University, where he was a Fulbright scholar. His work is focused on solid state research at extreme conditions.

Andrzej Grzechnik

Karen Friese studied mineralogy (Diploma) at the University of Hamburg, where she also obtained her PhD. Her work is focused on crystal structure determination of functional materials.

Karen Friese

apart from V_7O_{13}, undergo metal–insulator phase transitions (MIT) accompanied by structural transformations.[6–10] *Magnéli* phases are also known for titanium, niobium, and tungsten oxides.[11]

The emphasis of this article is on the homologous series of vanadium oxides V_nO_{2n+1} predicted by A. D. Wadsley[12] in the system V_2O_5–VO_2. Its formula can be written as V_nO_{2n+1} = $V_2O_5 + (n - 2)$ VO_2 for $2 \leq n$. The end members of this homologous series are α-V_2O_5 (*Pmmn*, $Z = 2$) and VO_2(B) (*C2/m*, $Z = 8$).[8] With respect to the chemical composition of VO_2, the Wadsley oxides are cation deficient, $V_{1-z}O_2$. They exhibit a variety of crystal structures due to different coordination polyhedra around the V atoms (tetrahedra, trigonal prisms, square pyramids, or octahedra) and different polyhedral connectivities. The V^{5+} cations favor the polyhedra with low coordination numbers, while the V^{4+} cations are five- or six-fold coordinated to the oxygen atoms.[13] Compared to the *Magnéli* phases, the polymorphism in the Wadsley series is altogether richer at ambient pressure. It offers a possibility to study the structure–property relationship in correlation with phase transitions including those induced at extreme conditions. In the following, the crystal structures and physical properties of the Wadsley homologous series V_nO_{2n+1} and of the relevant polymorphs of vanadium dioxide are reviewed. It is then indicated how high-pressure phase transitions and synthesis could lead to new materials in the V_2O_5–VO_2 system.

Rutile-type and VO$_2$(S) vanadium dioxides

The first-order MIT in stoichiometric vanadium dioxide occurs at $T_{MIT} \approx 341$ K.[14–17] It is associated with a magnetic susceptibility drop and a change in thermochromic properties. The V^{3+} and V^{5+} cations co-exist in the high-temperature metallic phase R due to charge fluctuations of the V^{4+} cations.[16] The V–V distance in the octahedral chains is equal to the c lattice parameter (Fig. 1). The low-temperature insulating phase M1 (*P2$_1$/c*, $Z = 4$) is made of VO_6 chains but with V–V dimers in a zigzag pattern due to displacement of the V atoms from the ideal-rutile positions.[18]

Doping with low-valence cations (*e.g.*, Al^{3+}, Cr^{3+}, Fe^{3+}) stabilizes additional insulating polymorphs M2 (*C2/m*, $Z = 8$) and T (*P1̄*, $Z = 4$). In M2, there are alternating short and long

V–V distances in the linear octahedral chain and equidistant V–V distances in the zigzag octahedral chain (Fig. 1).[19,20] T is a distorted variant of M2 due to linearity breaking and pairing of the V atoms in the zigzag chain.[20] M1 and M2 can transform into each other, with T as an intermediate.[19] M2 can also be an intermediate in the M1 → R transition.[21–23] The three insulating phases may coexist and form domains.[24] Their stabilities are affected by electric field, strain, or pressure.[14,16,25,26] The high-valence dopants (*e.g.*, Nb^{5+}, Mo^{6+}, W^{6+}) lower T_{MIT}, while the low-valence dopants (*e.g.*, Al^{3+}, Cr^{3+}, Fe^{3+}) increase it.[14–16] The charge is compensated by the presence of the V^{3+} or V^{5+} cations, respectively. In non-stoichiometric undoped vanadium dioxide, T_{MIT} decreases in VO_{2-y} with increasing y, while it increases in $V_{1-z}O_2$ with increasing z.[15–17] The crystallographic data across MIT for different non-stoichiometries are lacking.[16]

In addition to the R and M1 polymorphs, insulating M1′ (monoclinic), metallic X (triclinic) and O (*Pnnm*, $Z = 4$) phases are identified in the pressure–temperature phase diagram of VO_2.[27] At room temperature, M1 transforms to isostructural M1′ at 13.9 GPa.[26] At 383 K, R undergoes a phase transition to O above 13.7 GPa.[28] Upon further compression, both M1′ and O transform into X above 34.3 and 38.3 GPa at room temperature and 383 K, respectively. X, which is postulated to be metallic above about 35 GPa,[28–31] co-exists with M1′ in the pressure range 32–42 GPa.

Insulating VO_2(S) (*P3*, $Z = 7$), synthesized from a mixture of V_2O_3 and V_2O_5 at 2–7 GPa and 873–1173 K, is built of isolated and strongly distorted edge-sharing octahedral VO_6 trimers arranged in two different layers.[32] The trimers in every second layer are linked *via* edge-sharing with another octahedron. Upon heating, the product transforms to M1 below 4 GPa and to M2 at higher pressures.

Cation-deficient $V_{1-z}O_2$ phases with a distorted rutile structure (*P2/m*, $Z = 2$) are synthesized at 6.5 GPa and 1273 K by substituting 2 wt% and 10 wt% of V_2O_5 into VO_2.[33,34] Their compositions could also be written as $V_{0.995}O_2$ and $V_{0.976}O_2$, respectively. The V–V distances in both octahedral chains are equidistant. The resistivity data show that $V_{0.995}O_2$ and $V_{0.976}O_2$ undergo MIT at 353 K and 361 K, respectively.[33] No structural details of the metallic phases in both materials are provided.

A summary of the compounds discussed in this section, including their space group symmetries, synthesis methods, V–V distances, and properties, is provided in Table S1 in the SI. Further details on polymorphism and physical properties of vanadium dioxide can be found in the ref. 2–5 and 14–17.

α-V$_2$O$_5$ and VO$_2$(B) end members of the Wadsley homologous series V$_n$O$_{2n+1}$

α-V$_2$O$_5$

α-V_2O_5 (*Pmmn*, $Z = 2$) is built of ribbons of edge-sharing VO_5 square pyramids or very distorted VO_6 octahedra when an additional long V–O distance is considered (Fig. 2).[13] The smallest building block in the idealized octahedral structure
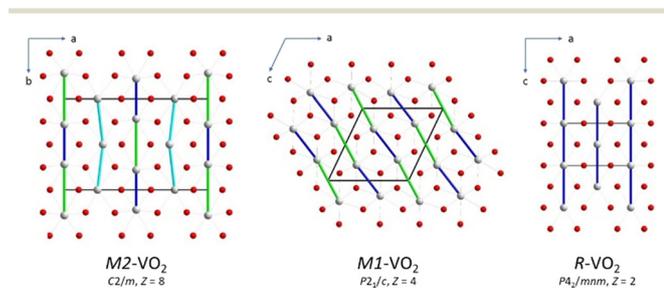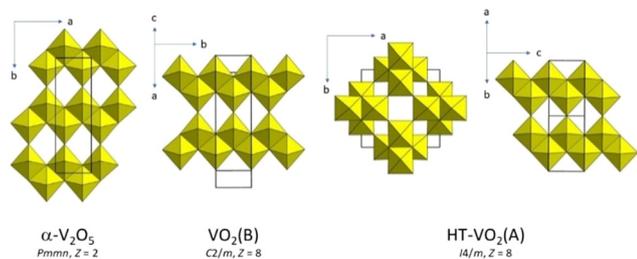

Fig. 1 Interatomic connectivity in VO_2 polymorphs. The V–V distances in the octahedral chains are drawn as thick green, blue, and cyan lines.

Below the figure:

M2-VO$_2$ / *C2/m, Z = 8*

M1-VO$_2$ / *P2$_1$/c, Z = 4*

R-VO$_2$ / *P4$_2$/mnm, Z = 2*

Fig. 2 Octahedral connectivity in the idealized α-V_2O_5 structure with distorted VO_6 octahedra, single layer in VO_2(B), and high-temperature phase of VO_2(A).

is a doublet of edge-sharing octahedra in the ribbons along the a axis. These ribbons are linked with the adjacent ones by corners to form layers. In each ribbon, there is a zigzag chain of equidistant V–V atoms.[35] The layers share corners in a three-dimensional structure.

α-V_2O_5 amorphizes above about 7.3 GPa.[36,37] The polymorph that crystallizes from the amorphous material at high pressures and high temperatures is δ-V_2O_5 ($C2/c$, $Z = 4$) as evidenced by *in situ* angle-dispersive synchrotron powder diffraction in large-volume multi-anvil press.[37] It is built of slabs connected with each other by octahedral corners.[36–39] Each slab is made of edge-sharing VO_6 doublets linked with the others by corners. The single slab is in fact a building block of the rutile type (Fig. 3). In β-V_2O_5 ($P2_1/m$, $Z = 2$), obtained at lower pressures than δ-V_2O_5,[38,39] there are two symmetry non-equivalent V positions V1 and V2. The octahedra $V1O_6$ form isolated stripes of the α-V_2O_5 type along the b direction. The $V2O_6$ octahedra are linked by corners to form chains along b. The stripes and chains share edges within one layer. The phase boundaries between α-V_2O_5 and the recovered β-V_2O_5 and δ-V_2O_5 products from high pressures and temperatures are drawn in ref. 39.

VO_2(B)

VO_2(B) is synthesized by reducing V_2O_5 in a sulphur or hydrogen atmosphere.[41] Its crystal structure ($C2/m$, $Z = 8$) consists of sheets of edge- and corner-sharing distorted VO_6 octahedra. It could be derived from the one of α-V_2O_5 by a crystallographic shear when every second oxygen plane is
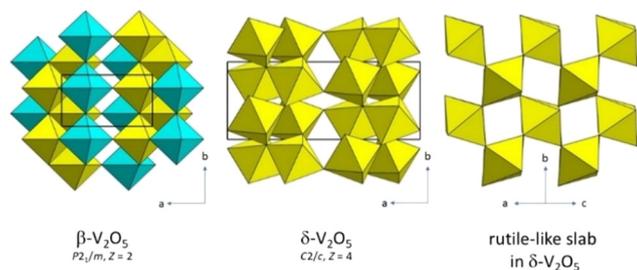
Fig. 3 High-pressure high temperature phases of V_2O_5. The $V1O_6$ and $V2O_6$ octahedra in β-V_2O_5 are drawn yellow and cyan, respectively.

removed, and the adjacent blocks are shifted by the vector $\frac{1}{6}[103]$. In an alternative description, each sheet in VO_2(B) could be separated into two layers of the idealized α-V_2O_5 type,[13] which share octahedral edges with each other (Fig. 2).

VO_2(B) as a bulk, nanorod, or thin film material undergoes a first-order isostructural phase transition in the range 180–300 K (ref. 42–46) with co-existing low-temperature (insulating and magnetically ordered), intermediate-temperature (insulating), and high-temperature (presumably metallic) phases.[45] The transition is associated with partial V^{4+}–V^{4+} pairing.[42] When heated in argon, it transforms to R.[43] When heated under reducing conditions, it turns into corundum. Annealing in vacuum yields M1.[47]

Under uniaxial tensile strain, VO_2(B) undergoes MIT at room temperature.[48] The transition along the b axis is gradual, while it is abrupt along the a axis. Insulating domains develop with increasing tensile strain along the b axis. They are due to the V–V dimerization within the distorted zigzag chains of vanadium atoms in the octahedral ribbons (Fig. 2).

The structural phase transition VO_2(B) → VO_2(A) is induced by uniaxial compressing and grinding VO_2(B) powders at room temperature and by subsequent heat treatment.[49,50] In nanobelts, the sequence of the phase transitions is VO_2(B) → VO_2(A)$_{HT}$ → VO_2(A)$_{LT}$, where VO_2(A)$_{LT}$ and VO_2(A)$_{HT}$ are the low- ($P4/ncc$, $Z = 16$) and high-temperature ($I4/m$, $Z = 8$) phases of VO_2(A), respectively.[51] In the low-temperature structure below 435 K, the V atoms form zigzags with alternating short and long V–V distances in the c direction due to V^{4+}–V^{4+} pairing. At higher temperatures, they form straight lines of equidistant V atoms. VO_2(A) has a lower formation energy compared to VO_2(B).[52] On annealing, VO_2(A) transforms to M1.[3]

The difference between VO_2(B) and both phases of VO_2(A) is the connectivity of the VO_6 octahedra (Fig. 2). According to the structure interpretation in ref. 48–51, the ribbons in VO_2(B) are formed by octahedral doublets that share edges with the adjacent doublets. In VO_2(A), the neighbouring doublets are rotated by 90° with respect to each other and share edges. The resulting chains share corners in the three-dimensional framework. Our description of the low- and high-temperature VO_2(A) structures, which is an alternative to the one in ref. 49–51, is that they consist of slabs of edge-sharing octahedra stacked along the [110] or [1$\bar{1}$0] directions. Each slab is then formed by two edge-sharing layers that are formed by ribbons that are nearly exactly like those in α-V_2O_5 and VO_2(B) (Fig. 2). In other words, α-V_2O_5, VO_2(B), and VO_2(A) have the same building unit that is the single layer of the idealized α-V_2O_5 octahedral type.[13] The differences arise from the stacking of these layers due to corner-sharing in α-V_2O_5 and different schemes of octahedral edge-sharing in VO_2(B) and VO_2(A).

At room temperature, VO_2(B) nanosheets and nanobelts become amorphous above 21 GPa (ref. 53) and 30 GPa,[54] respectively, due to a dynamically hindered transformation to M1.[53] When annealed at atmospheric pressure, the recovered

material, produced during amorphization of the nanosheets, recrystallizes back to $VO_2(B)$. $VO_2(A)$ becomes metallic at about 28 GPa and amorphizes at 32 GPa at room temperature.[55]

Wadsley homologous series V_nO_{2n+1}

Known Wadsley V_nO_{2n+1} phases are V_3O_7 ($V_{0.86}O_2$), V_4O_9 ($V_{0.89}O_2$), and V_6O_{13} ($V_{0.92}O_2$) (Fig. 4). The stable compounds in the experimentally determined V–O phase diagram are V_3O_7 and V_6O_{13},[1] while thermodynamical calculations find only V_3O_7 as a stable phase.[2] The difficulty extending the series using various synthesis methods at ambient conditions is due to different chemical and structural characteristics of the V^{4+} and V^{5+} cations. The unifying description of the crystal structures for n = 2, 3, and 6 as well as for α-V_2O_5 and $VO_2(B)$ is presented in ref. 8. These materials have oxygen-deficient structures deduced from VO_x ($Fm\bar{3}m$, Z = 4), where $x \approx 1$, by introducing different ordered vacancies in the oxygen close-packing array. Symmetry breaking and collapse of the fcc layers along the cubic c axis induces shear deformations. The considerations in ref. 8 do not include the analysis of the structures of V_4O_9 determined in ref. 56 and 57. A classification of the polyhedral connectivities is given in ref. 13. A summary of the compounds discussed in this section, including α-V_2O_5 as well as $VO_2(B)$ and $VO_2(A)$, is provided in Table S2 in the SI.

V_3O_7

V_3O_7 ($C2/c$, Z = 12), which is an insulator and uniaxial ferromagnet,[58,59] is synthesized from a mixture of V_2O_3 and V_2O_5.[60] The structure is built of distorted VO_6 octahedra and VO_5 polyhedra joined by corner- and edge-sharing to form a three-dimensional framework (Fig. 4). The VO_5 polyhedra could be interpreted either as distorted trigonal bipyramids or square pyramids. The V^{4+} cations are situated in the octahedra, while the V^{5+} cations are in the VO_5 polyhedra.

Related to $VO_2(S)$[32] is the cation-deficient insulating oxide $V_{3.047}O_7$ ($P3$, Z = 2) obtained by reduction of V_2O_5 at 5 GPa and 1073 K.[61] It has a composition very close to V_3O_7 and is reported to have the $Al_4Ta_3O_{13}(OH)$ simpsonite-type structure. The structure of $V_{3.047}O_7$ is described as a stacking of two octahedral layers along the c direction. One of them has isolated triplets of edge-sharing VO_6 octahedra. In the other, the triplets are connected to each other *via* additional bridging octahedra around partially occupied vanadium sites. Zibr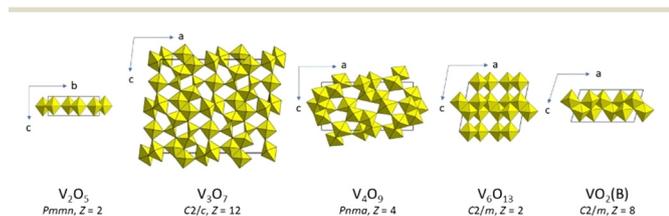ov *et al.*[61] expected that a new phase of V_3O_7 with the simpsonite structure could also be synthesized from a mixture of V_2O_3 and V_2O_5 at the same pressure–temperature conditions. However, their synthesis was not successful.

V_4O_9

Three different V_4O_9 products, depending on the synthesis procedures, are reported in the literature. The phase prepared by decomposing V_3O_7 in supercritical water at 873 K and 0.2 GPa ($Pnma$, Z = 4) is built of highly distorted edge-sharing octahedra in zigzag ribbons running along the b direction (Fig. 4).[56] The ribbons are joined by corners to form a three-dimensional framework. V_4O_9 could also be grown topotactically on single crystals of α-V_2O_5 by reducing them in a sulphur atmosphere.[57] The resulting crystal structure can then be considered a distorted superstructure of α-V_2O_5. The third product ($Cmcm$, Z = 8) can be obtained with a soft chemistry method also by reducing V_2O_5 with sulphur.[62] It is composed of pairs of distorted edge-sharing octahedra and square pyramids linked by corner sharing with tetrahedra. The V atoms in the octahedra and pyramids have the valence 4+, while they have the valence 5+ in the tetrahedra. Such a structure cannot be explained with the shear concept that relies on the presence of oxygen-plane faults. This product is a spin-$\frac{1}{2}$ one-dimensional antiferromagnetic system with a spin-gap ground state.[62]

α-V_6O_{13}

α-V_6O_{13} ($C2/m$, Z = 2), obtained by reacting a mixture of V_2O_3 and V_2O_5 in an evacuated quartz glass tube at 873 K,[63–65] is composed of single and double layers formed by edge- and corner-sharing distorted VO_6 octahedra. The crystal structure can be described as built of alternating $VO_2(B)$- and idealized α-V_2O_5-like layers stacked along the c axis (Fig. 2, 4, and 5). One of the sites for the vanadium atoms in the double layer is preferentially occupied by the V^{5+} cations.[66] In the idealized α-V_2O_5, the shear planes separate narrow slabs of the ReO_3 type.[65] The structure of α-V_6O_{13} is formed when another set of shear planes, perpendicular to the first, is introduced in α-V_2O_5 resulting in the loss of oxygen. The relationship between α-V_2O_5 and α-V_6O_{13} is also defined in ref. 67. Removing all the atoms on every third (001) oxygen-atom plane in α-V_2O_5 and introducing crystallographic shear $\frac{1}{6}[10\bar{3}]$ leads to the structure of α-V_6O_{13}. Such a mechanism of transformations yields the double layer of the $VO_2(B)$ type.

Fig. 4 Idealized crystal structures in the Wadsley homologous series.

V_2O_5
$Pmmn$, Z = 2

V_3O_7
$C2/c$, Z = 12

V_4O_9
$Pnma$, Z = 4

V_6O_{13}
$C2/m$, Z = 2

$VO_2(B)$
$C2/m$, Z = 8
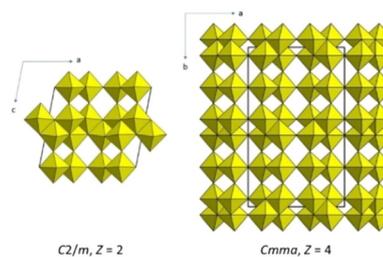
Fig. 5 Crystal structures of the α and β phases of V_6O_{13}.

$C2/m$, Z = 2

$Cmma$, Z = 4

The shear in β-V_6O_{13} (*Cmma*, $Z = 4$), which is obtained by exposure of α-V_6O_{13} to an electron beam[67] and by hydrothermal synthesis,[68] is $\frac{1}{2}[0\bar{1}\bar{1}]$. The difference between the α and β phases of V_6O_{13} is clearly visible in Fig. 5: the double layer in β is like the slab in VO_2(A) (Fig. 2). Worth noting is the fact that a pseudosymmetry search[69] in β-V_6O_{13} with respect to the minimal supergroups of *Cmma* results in the structure with space group *Fmmm* ($Z = 4$). This transformation does not involve any atomic displacements indicating that the reported space group symmetry *Cmma*[67] is too low.

α-V_6O_{13} is a paramagnetic metal at ambient conditions. It undergoes MIT at $T_{MIT} = 150$ K but remains paramagnetic down to 55 K.[70–75] T_{MIT} decreases to 100 K at 1.4 GPa.[74] The low-temperature crystal structure is disputed as $C2$ (ref. 74) and $P2_1/a$[76] space groups are initially proposed. The most recent study reports the structure in space group *Pc*.[70] All these models exhibit a high degree of pseudosymmetry with respect to space group $C2/m$ and distortions from the parent phase are very small. In *Pc*, all the atoms are displaced from the mirror plane, but the structural changes appear mainly in the single layer. The charge transfer between the vanadium atoms in the single and double layers takes place during this phase transition. Some of the vanadium atoms in the single layer acquire more pentavalent character, while the others develop the tetravalent one. The model in space group *Pc* is then used to explain the changes of various physical properties across MIT in all subsequent studies.[71–74] At $T_N \approx$ 55 K, α-V_6O_{13} becomes antiferromagnetically ordered.[74] However, the crystal and magnetic structures below T_N have not been reported yet.

At room temperature, α-V_6O_{13} is structurally stable to at least 9.4 GPa.[37] Single-crystals of rutile-related $V_{0.92}O_2$ can be grown at 10 GPa and 1273 K from a polycrystalline α-V_6O_{13} starting material.[65] *In situ* synchrotron measurements reveal that this new phase starts to crystallize above 500 K in the pressure range 4–17.5 GPa and is recovered to ambient conditions. The characteristic feature of its crystal structure ($C2/m$, $Z = 4$) is the presence of disorder affecting the V atoms, which occupy two split atom positions V1 and V2 (Fig. 6). The V1 atoms in one of the octahedral chains are
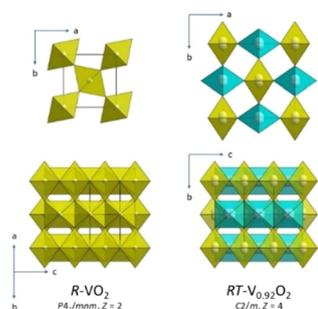
displaced along the *b* axis, while the V2 atoms in the other are four-fold split in the (b, c) plane. This results in two zigzag V–V chains: one with equidistant V1 atoms and the other with short and long V2–V2 distances. There is no indication for V^{4+} and V^{5+} charge ordering and separation. Disregarding the V split positions, the average structure ($P2/m$, $Z = 2$) of this new phase is like the one for the $V_{1-z}O_2$ material obtained by Chamberland.[33,34] Pseudo-symmetry considerations[69] indicate that rutile-related $V_{0.92}O_2$ is a variant of insulating M2 (Fig. 1).[65]

$V_{0.92}O_2$ is metastable when recovered to ambient conditions. It starts to decompose at 470 K and atmospheric pressure.[77] At about 350 K, the material undergoes a first-order phase transition, in which the low- and high-temperature phases have the same average structure ($P2/m$, $Z = 2$). The temperature for this transformation correlates well with those in $V_{0.995}O_2$ and $V_{0.976}O_2$.[33] $V_{0.92}O_2$ above the phase transition forms a modulated structure in super-space group $X2/m(0\beta0)s0$ ($Z = 2$) with the centering vector $X(\frac{1}{2}, 0, \frac{1}{2}, \frac{1}{2})$. The structure is remarkable as it is mainly the modulation of the displacement parameters of the vanadium atoms that dominate the incommensurate phase. Both structures of $V_{0.92}O_2$ have one important feature common to all the known (non-)stoichiometric VO_2 phases: the hexagonal close-packing oxygen sublattice is rigid while the cation sublattice is flexible, allowing for various schemes of cation (dis)order.

The first-order phase transition to the incommensurate phase in $V_{0.92}O_2$ is also visible in the temperature-dependent resistivity data measured on a single crystal on heating and cooling in the range 275–400 K.[77] On heating, the onset of the phase transition is at about 330 K. A hysteresis of about 10 K is observed on cooling the crystal from 400 K down to room temperature. Both phases of $V_{0.92}O_2$ are insulating. Such a behaviour is different from that of (nearly) stoichiometric VO_2, in which the high-temperature phases are metallic.[16,32]

On compression at room temperature, $V_{0.92}O_2$ reaches the ideal rutile structure at about 5.0 GPa.[77] This transformation is also of the first-order character. It demonstrates that the structural behavior of the cation deficient vanadium dioxide at extreme conditions is distinctly different from that of stoichiometric VO_2.[26–31]

Conclusions and outlook

Ribbons of edge-sharing VO_6 octahedral doublets could be traced in the crystal structures along the Wadsley series at atmospheric pressure. They are a basic building unit in idealized α-V_2O_5, VO_2(B), and related VO_2(A). The connectivity of the rutile type, with chains of edge-sharing octahedra joined with each other by corners, can be found in the materials synthesized at high pressures. It is partially realized in δ-V_2O_5 (ref. 37–40) and fully achieved in $V_{0.92}O_2$ (ref. 65 and 77) obtained from V_6O_{13}. This could imply that vanadium oxides with the Wadsley stoichiometries V_nO_{2n+1} and high VO_2 content (at least $n \geq 6$) would tend to

Fig. 6 Comparison of the ideal rutile and $V_{0.92}O_2$ crystal structures. The $V1O_6$ and $V2O_6$ octahedra are drawn yellow and cyan, respectively.

transform to the rutile type at extreme conditions. The crystal structures of the *Magnéli* phases at ambient are also derived from the rutile one. The rutile structure would then be an aristotype for both cation and anion deficient vanadium dioxides at various pressures and temperatures. The rigidity of the hexagonal close-packing oxygen sublattice and different occupational schemes of the V^{3+}, V^{4+}, and V^{5+} cations could also result in the occurrence of incommensurate phases in non-stoichiometric VO_2.

Metallic properties in all the rutile-type as well as Wadsley phases are observed in the compounds with no V–V dimerization along the octahedral chains (see also Tables S1 and S2 in the SI). The application of pressure in the synthesis could yield materials with shorter V–V distances but would not necessarily break the dimers. Based on the current data available for the V_2O_5–VO_2 system, it is not possible to establish any relation of the crystal structures and properties with the synthesis conditions without considering the compositional variations. $V_{0.92}O_2$, which is insulating, contains 35 wt% of V_2O_5.[65,77] It demonstrates the capacity of the rutile-type framework to accommodate a wide range of VO_2–V_2O_5 compositions. Varying stoichiometries and pressure–temperature conditions could then yield $V_{1-z}O_2$ materials with transport properties ranging from metallic to insulating. Since the compound with 10 wt% of V_2O_5 ($V_{0.976}O_2$) is indeed metallic,[33] it remains to be seen for which higher V_2O_5 contents $V_{1-z}O_2$ oxides would become insulating. In addition, 35 wt% of V_2O_5 does not need to be a compositional limit for the stability of the rutile-related structures. We conclude then that materials engineering by varying compositions in the system V_2O_5–VO_2 and exerting high pressures and temperatures offers a possibility to synthesize new materials with unexpected properties.

Previous studies show that T_{MIT} decreases in the anion-deficient VO_{2-y}, while it increases in the cation-deficient $V_{1-z}O_2$.[14,16,33] For small deviations from the exact VO_2 stoichiometry, the high-temperature phase is supposed to have the ideal rutile structure. However, this has not been clearly demonstrated either for the compounds synthesized at elevated pressures reported in ref. 33 nor for several materials, which can already be obtained at atmospheric conditions.[16] Further detailed investigations of the structural and electronic (in)stabilities in the non-stoichiometric vanadium dioxides are then warranted as the occurrence of the ideal R and metallic phases in the $V_{1-z}O_2$ materials is not demonstrated.

Author contributions

Both authors contributed equally to this work.

Conflicts of interest

No conflicts of interest.

Data availability

All data discussed in the manuscript are available upon request.

Supplementary information (SI) is available. See DOI: https://doi.org/10.1039/d5ce01171j.

Acknowledgements

Notes and references

1 H. A. Wriedt, *Bull. Alloy Phase Diagrams*, 1989, **10**, 271–277.

2 P. Hu, P. Hu, T. D. Vu, M. Li, S. Wang, Y. Ke, X. Zeng, L. Mai and Y. Long, *Chem. Rev.*, 2023, **123**, 4353–4415.

3 M. Li, S. Magdassi, Y. F. Gao and Y. Long, *Small*, 2017, **13**, 1701147.

4 O. Monfort and P. Petrisková, *Processes*, 2021, **9**, 214.

5 N. Vishwakarma, A. A. Remadevi, D. Kumar, A. Solanki, A. S. Rana and A. Srivastava, *J. Appl. Phys.*, 2024, **135**, 025303.

6 U. Schwingenschlögl and V. Eyert, *Ann. Phys.*, 2004, **13**, 475–510.

7 J. M. Allred and R. J. Cava, *J. Solid State Chem.*, 2013, **198**, 10–17.

8 H. Katzke, P. Tolédano and W. Depmeier, *Phys. Rev. B: Condens. Matter Mater. Phys.*, 2003, **68**, 024109.

9 S. Åsbrink, *Acta Crystallogr., Sect. B*, 1980, **36**, 1332–1339.

10 S.-H. Hong and S. Åsbrink, *Acta Crystallogr., Sect. B*, 1982, **38**, 713–719.

11 X. Wu, H. Wang and Y. Wang, *Materials*, 2023, **16**, 6874.

12 A. D. Wadsley, *Acta Crystallogr.*, 1957, **10**, 261–267.

13 P. Y. Zavalij and M. S. Whittigham, *Acta Crystallogr., Sect. B: Struct. Sci.*, 1999, **55**, 627–663.

14 J.-P. Pouget, *C. R. Phys.*, 2021, **22**, 37–87.

15 Y. Xue and S. Yin, *Nanoscale*, 2022, **14**, 1054–1097.

16 S. Joshi, N. Smieszek and V. Chakrapani, *Sci. Rep.*, 2023, **10**, 17121.

17 H. Sim, K.-Y. Doh, Y. Park, K. Song, G.-Y. Kim, J. Son, D. Lee and S.-Y. Choi, *Small*, 2024, **20**, 2402260.

18 J. M. Longo and P. Kierkegaard, *Acta Chem. Scand.*, 1970, **24**, 420–426.

19 M. Marezio, D. B. McWhan, J. P. Remeika and P. D. Dernier, *Phys. Rev. B: Solid State*, 1972, **5**, 2541–2551.

20 M. Ghedira, H. Vincent, M. Marezio and J. C. Launay, *J. Solid State Chem.*, 1977, **22**, 423–438.

21 M. Liu, S. Xie, L. Wei, M. Galluzzi, Y. Li, Q. Wang, X. Zhou, Y. Wang and J. Li, *Acta Mater.*, 2020, **195**, 720–727.

22 Y. Bleu, F. Bourquard, K. Misdanitis, A. Poulet, A.-S. Loir, F. Garrelie and C. Donnet, *Mater. Today Commun.*, 2023, **35**, 105564.

23 D. K. Manousou, S. B. Atata, Y. J. Sohn, P. Tsipas, A. Grzechnik, M. Calamiotou, K. Friese and S. Gardelis, *J. Alloys Compd.*, 2025, **1024**, 18081.

24 P. Lu, J. Zhou, X. Liu, Z. Zhang, F. Xu, L. Zhang, X. Mou, J. Feng, Y. Gao and J. Zhao, *J. Appl. Crystallogr.*, 2014, **47**, 732–738.

25 Z. Shao, X. Cao, H. Luo and P. Jin, *NPG Asia Mater.*, 2018, **10**, 581–605.

26 P. Bouvier, L. Bussmann, D. Machon, I. Breslavetz, G. Garbarino, P. Strobel and V. Dmitriev, *Phys. Rev. B*, 2023, **108**, 144106.

27 Y. Chen, S. Zhang, F. Ke, C. Ko, S. Lee, K. Liu, B. Chen, J. W. Ager, R. Jeanloz, V. Eyert and J. Wu, *Nano Lett.*, 2017, **17**, 2512–2516.

28 L. Bai, Q. Li, S. A. Corr, Y. Meng, C. Park, S. V. Sinogeikin, C. Ko, J. Wu and G. Shen, *Phys. Rev. B: Condens. Matter Mater. Phys.*, 2015, **91**, 104110.

29 H. Zhang, Q. Li, B. Cheng, Z. Guan, R. Liu, B. Liu, Z. Liu, X. Li, T. Cui and B. Liu, *RSC Adv.*, 2016, **6**, 104949–104954.

30 Q. Li, H. Zhang, C. Lin, F. Tian, J. S. Smith, C. Park, B. Liu and G. Shen, *J. Alloys Compd.*, 2017, **709**, 260–266.

31 H. Zhang, Q. Li, F. Wang, R. Liu, Y. Mao, Z. Liu, X. Li, K. Yang, T. Cui and B. Liu, *J. Phys. Chem. C*, 2019, **123**, 955–962.

32 I. P. Zibrov, V. P. Filonenko, V. A. Sidorov, N. M. Chtchelkatchev and M. V. Magnitskaya, *Materialia*, 2022, **23**, 101456.

33 B. L. Chamberland, *J. Solid State Chem.*, 1973, **7**, 377–384.

34 J. Galy and G. Miehe, *Solid State Sci.*, 1999, **1**, 433–448.

35 R. Enjalbert and J. Galy, *Acta Crystallogr., Sect. C: Cryst. Struct. Commun.*, 1986, **42**, 1467–1469.

36 A. Grzechnik, *Chem. Mater.*, 1998, **10**, 2505–2509.

37 B. V. Hakala, D. K. Manousou, K. Glazyrin, W. A. Crichton, K. Friese and A. Grzechnik, *J. Alloys Compd.*, 2022, **911**, 164966.

38 V. P. Filonenko, M. Sundberg, P. E. Werner and I. P. Zibrov, *Acta Crystallogr., Sect. B: Struct. Sci.*, 2004, **60**, 375–381.

39 P. Balog, D. Orosel, Z. Cancarevic, C. Schön and M. Jansen, *J. Alloys Compd.*, 2007, **429**, 87–98.

40 I. P. Zibrov, V. P. Filonenko, S. G. Lyapin and V. A. Sidorov, *High Pressure Res.*, 2013, **33**, 399–408.

41 F. Théobald, R. Cabala and J. Bernard, *J. Solid State Chem.*, 1976, **17**, 431–438.

42 Y. Oka, T. Yao, N. Yamamoto, Y. Ueda and A. Hayashi, *J. Solid State Chem.*, 1993, **105**, 271–278.

43 S. A. Corr, M. Grossman, Y. Shi, K. R. Heier, G. D. Stucky and R. Seshadri, *J. Mater. Chem.*, 2009, **19**, 4362–4367.

44 J. Lourembam, A. Srivastava, C. La-o-vorakiat, H. Rotella, T. Venkatesan and E. E. M. Chia, *Sci. Rep.*, 2015, **5**, 9182.

45 S. R. Popuri, A. Artemenko, R. Decourt, M. Josse, U. C. Chung, D. Michau, M. Maglione, A. Villesuzanne and M. Pollet, *J. Phys. Chem. C*, 2015, **119**, 25085–25092.

46 J. Lourembam, A. Srivastava, C. La-o-vorakiat, L. Cheng, T. Venkatesan and E. E. M. Chia, *Sci. Rep.*, 2016, **6**, 25538.

47 S. R. Popuri, M. Miclau, A. Artemenko, C. Labrugere, A. Villesuzanne and M. Pollet, *Inorg. Chem.*, 2013, **52**, 4780–4785.

48 Z. Ma, S. Yan, Z. Liu, T. Xu, F. Chen, S. Chen, T. Cao, L. Sun, B. Chen, S.-J. Liang and F. Miao, *Chin. Phys. B*, 2024, **33**, 067103.

49 Y. Oka, T. Yao and N. Yamamoto, *J. Solid State Chem.*, 1990, **86**, 116–124.

50 Y. Oka, T. Yao and N. Yamamoto, *J. Mater. Chem.*, 1991, **1**, 815–818.

51 Y. Oka, S. Sato, T. Yao and N. Yamamoto, *J. Solid State Chem.*, 1998, **141**, 594–598.

52 S. Zhang, B. Shang, J. Yang, W. Yan, S. Wei and Y. Xie, *Phys. Chem. Chem. Phys.*, 2011, **13**, 15873–15881.

53 Y. Wang, J. Zhu, W. Yang, T. Wen, M. Pravica, Z. Liu, M. Hou, Y. Fei, L. Kang, Z. Lin, C. Jin and Y. Zhao, *Nat. Commun.*, 2016, **7**, 12214.

54 B. Cheng, H. Zhang, Q. Li, J. Liu and B. Liu, *Inorganics*, 2022, **10**, 122.

55 B. Cheng, Q. Li, H. Zhang, R. Liu, B. Liu, Z. Yao, T. Cui, J. Liu, Z. Liu, B. Sundqvist and B. Liu, *Phys. Rev. B*, 2016, **93**, 184109.

56 K.-A. Wilhelmi and K. Waltersson, *Acta Chem. Scand.*, 1970, **24**, 3409–3411.

57 G. Grymonprez, L. Fiermans and J. Vennik, *Acta Crystallogr., Sect. A*, 1977, **33**, 834–837.

58 A. Heidemann, K. Kosuge, Y. Ueda and S. Kachi, *Phys. Status Solidi A*, 1977, **39**, K37.

59 H. Nishihara, Y. Ueda, K. Kosuge, H. Yasuoka and S. Kachi, *J. Phys. Soc. Jpn.*, 1979, **47**, 790.

60 K. Waltersson, B. Forslund and K.-A. Wilhelmi, *Acta Crystallogr., Sect. B*, 1974, **30**, 2644–2652.

61 I. P. Zibrov, V. P. Filonenko, V. A. Sidorov and S. G. Lyapin, *Inorg. Mater.*, 2016, **52**, 902–908.

62 S. Yamazaki, C. Li, K. Ohoyama, M. Nishi, M. Ichikara, H. Ueda and Y. Ueda, *J. Solid State Chem.*, 2010, **183**, 1496–1503.

63 K. Kawashima, Y. Ueda, K. Kosuge and S. Kachi, *J. Cryst. Growth*, 1974, **26**, 321–322.

64 Y. Ueda, K. Kosuge and S. Kachi, *Mater. Res. Bull.*, 1976, **11**, 293–298.

65 A. Grzechnik, B. V. Hakala, S. Kurig, N. Walte, N. Tsujino, S. Kakizawa, Y. Higo, D. Zagorac, J. Zagorac, R. Dronskowski, J. C. Schön and K. Friese, *Cryst. Growth Des.*, 2024, **24**, 5582–5592.

66 K.-A. Wilhelmi, K. Waltersson and L. Kihlborg, *Acta Chem. Scand.*, 1971, **25**, 2675–2687.

67 T. Ohno, Y. Nakamura and S. Nagakura, *J. Solid State Chem.*, 1985, **56**, 318–324.

68 Y. Zhang and C. Meng, *Mater. Lett.*, 2015, **160**, 404–407.

69 C. Capillas, E. S. Tasci, G. de la Flor, D. Orobengoa, J. M. Perez-Mato and M. I. Aroyo, *Z. Kristallogr.*, 2011, **226**, 186–196.

70 J. Höwing, T. Gustafsson and J. O. Thomas, *Acta Crystallogr., Sect. B: Struct. Sci.*, 2003, **59**, 747–752.

71 Y. Shimizu, S. Aoyama, T. Jinno, M. Itoh and Y. Ueda, *Phys. Rev. Lett.*, 2015, **114**, 166403.

72 M. Onoda, T. Ohki and Y. Uchida, *J. Phys.: Condens. Matter*, 2004, **16**, 7863–7871.

73 T. Toriyama, T. Nakayama, T. Konishi and Y. Ohta, *Phys. Rev. B: Condens. Matter Mater. Phys.*, 2014, **90**, 085131.

74 I. V. Leonov, *JETP Lett.*, 2022, **116**, 884–890.

75 P. D. Dernier, *Mater. Res. Bull.*, 1974, **9**, 955–964.

76 I. Kawada, I. Motohiko, M. Saeki, N. Kimizuka, M. Nakano-Onoda and K. Kato, *Acta Crystallogr., Sect. B*, 1978, **34**, 1037–1039.

77 A. Grzechnik, V. Petříček, P. Reiss, P. Zakalek, D. Chernyshov and K. Friese, *IUCrJ*, 2026, **13**, 116–125.